there results from Eq. (1)

$$\varepsilon = \tau_{12} + \tau_{13} \tag{3}$$

Through the consideration of energy balance and mirror image (Fig. 1), it can be established that

$$\tau_{12} = \tau(L_0) - \rho\tau(2L_0) \tag{4}$$

and

$$\tau_{13} = 1 - (1-\rho)\tau(L_0) - \rho\tau(2L_0) \tag{5}$$

where L_0 (aspect ratio) $= L/h$ and ρ is the hemispherical specular reflectance of cavity walls. Thus, the apparent emittance can be simply expressed as

$$\varepsilon = 1 - \rho[2\tau(2L_0) - \tau(L_0)] \tag{6}$$

and evaluated by substituting the numerical values of transmittance reported by Edwards and Tobin.[2]

Figure 2 presents the results for the apparent emittance of rectangular groove cavities with specularly reflecting metallic walls. Results for the case of dielectric walls can also be obtained in a similar manner. The effect of polarization is illustrated by the comparison in Fig. 2 between the present results and those of Sparrow and Jonsson[4] who neglected polarization in their calculation. It is clearly indicated that the polarization effect is indeed significant in this case.

References

[1] Edwards, D. K. and Bevans, J. T., "Effect of Polarization on Spacecraft Radiation Heat Transfer," *AIAA Journal*, Vol. 3, 1965, p. 1323.

[2] Edwards, D. K. and Tobin, R. D., "Effect of Polarization on Radiant Heat Transfer through Long Passages," *Journal of Heat Transfer*, 89C, 1967, pp. 132–138.

[3] Toor, J. S., Viskanta, R., and Winter, E. R. F., "Effects of Polarization on Radiant Heat Interchange Between Singly Arranged Surfaces," *AIAA Journal*, Vol. 8, No. 5, May 1970, pp. 981–983.

[4] Sparrow, E. M. and Jonsson, V. K., "Thermal Radiation Absorption in Rectangular-Groove Cavities," *Journal of Applied Mechanics*, 85E, 1963, pp. 237–244.

[5] Sparrow, E. M. and Cess, R. D., *Radiation Heat Transfer*, revised edition, Brooks/Cole, Belmont, Calif., 1970.

Effect of Ground Wind Shear on Aircraft Trailing Vortices

DAVID C. BURNHAM*

U. S. Department of Transportation, Cambridge, Mass.

THE motion of the pair of trailing vortices generated by an aircraft is not well described by simple line vortex theory in the presence of a cross wind near the ground. Experimental observations indicate that the up-wind vortex usually drops to a lower altitude than the down-wind vortex. Figure 1 shows a photograph of this phenomenon where the vortex locations are marked by smoke from a tower. Figure 2 shows typical vortex trajectories measured with a pulsed acoustic ranging system developed at this center.

The standard way of calculating the effect of a cross wind on the vortex motion is to add the horizontal wind velocity to the normal[1] induced motion of the vortices. According to this description. the two vortices always remain at equal altitudes. This treatment is inadequate because it neglects the vorticity which is present in the wind shear layer near the ground.

In order to understand the observed asymmetry in vortex height, a self-consistent two-dimensional calculation was made of the vortex motion for a simple model in which all the vorticity

Received February 22, 1972; revision received April 10, 1972.

Index category: Jets, Wakes, and Viscid-Invicid Flow Interactions.

* Staff Scientist, Transportation Systems Center.

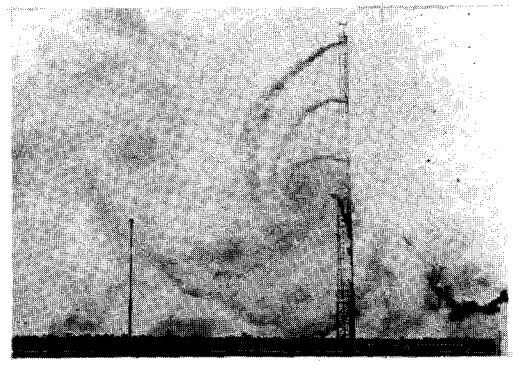

Fig. 1 Photograph of a vortex pair with smoke visualization; note wind direction and upward displacement of vortex on the left. (Courtesy of the Federal Aviation Administration.)

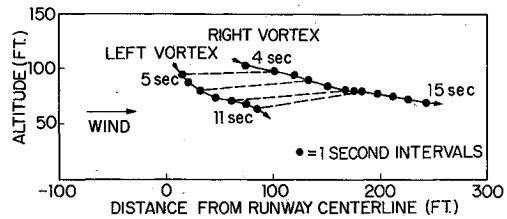

Fig. 2 Trajectories of vortices generated by a B-727 approaching Logan International Airport, runway 22L.

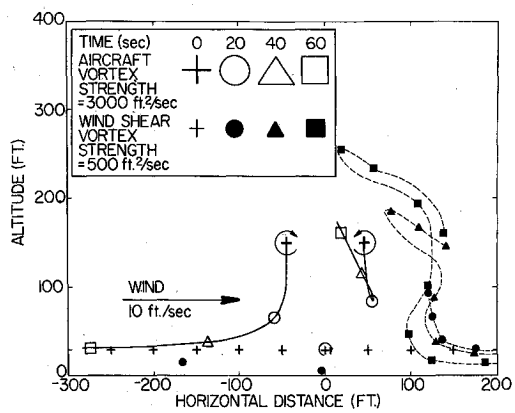

Fig. 3 Calculated vortex trajectories in the frame of reference moving with the wind; 21 wind shear vortices were initially located at 30 ft altitude and 50 ft intervals between −400 and +600 ft.

of the ground shear layer is concentrated into a series of evenly spaced line vortices at a particular altitude. Although this model leads to an unrealistic wind field near each wind shear vortex, it will give a reasonable description of winds at distances larger than the vortex spacing ΔX. In particular, the high altitude (i.e. altitude $\gg \Delta X$) wind is given by the expression $V = \Gamma/\Delta X$ where Γ is the strength (circulation) of each wind shear vortex. In the calculation all vortices above the ground (altitude Y) were paired with oppositely rotating image vortices (altitude ϕY) in order to satisfy the boundary condition of no vertical wind at the ground. The induced motion of each vortex by all the other vortices was then evaluated in order to find the vortex trajectories. The computer time required to carry out this procedure is proportional to $mn(n-1)$ where m is the number of time increments and n is the total number of vortices. Because of this restriction, a rather coarse grid of points was used. The horizontal extent of the wind shear vortices was made large enough that end effects could be ignored without introducing drastic errors in the region near the aircraft vortices.

The results of one such calculation are shown in Fig. 3 where the aircraft vortex parameters are those corresponding to a

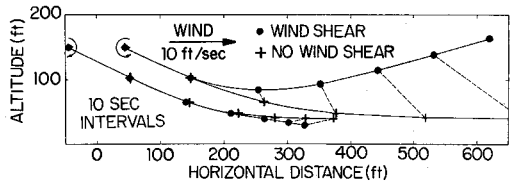

Fig. 4 Calculated vortex trajectories in the ground frame of reference.

B-727 aircraft. In the frame of reference moving with the wind, the wind shear vortices normally move at half the wind speed in the direction opposite to the wind (i.e., 5 fps to the left in Fig. 3). The effect of the aircraft vortices on this motion is to speed it up on the up-wind side and to reverse it on the down-wind side. The wind shear vortices approaching from the right in Fig. 3 are swept up in the air and eventually induce the down-wind vortex to reverse its downward motion and move back up. After 60 sec, this vortex has captured wind shear vorticity of equal magnitude to its own and is moving upward at a speed comparable to its initial downward motion. The up-wind vortex, on the contrary, finds itself isolated from wind shear vorticity and therefore is influenced only by its image vortex. These motions are shown in Fig. 4 in the ground frame of reference. For comparison, the trajectories for a uniform wind are also shown. The trajectory of the up wind vortex is almost the same for the two cases, as one might expect.

Although the model used here is crude, it gives a qualitative description of the observed difference in the motion of the two vortices. The effect is similar to but stronger than that proposed by Harvey and Perry[1] to explain the rising of vortices. It should be noted that the effect discussed in this note is actually produced by the vertical gradient in the wind shear rather than by the wind shear directly. One can easily see that the wind shear vortices would not affect the aircraft vortex vertical motion at all if they were uniformly distributed in space.

The phenomenon described in this Note pertains to relatively low cross winds. Both experimental observations and calculations indicate that other phenomena occur at much higher cross wind speeds (e.g. 30 fps instead of the 10 fps considered here).

Reference

[1] Harvey, J. K. and Perry, F. J., "Flowfield Produced by Trailing Vortices in the Vicinity of the Ground," *AIAA Journal*, Vol. 9, No. 8, Aug. 1971, pp. 1659–1660.

Three-Dimensional Structure and Equivalence Rule of Transonic Flows

H. K. Cheng* and Mohammed Hafez†
University of Southern California, Los Angeles, Calif.

Introduction

For smooth configurations of very low aspect ratio, a theoretical basis of Whitcomb's transonic area rule[1] has been established by Oswatish and Keune[2] and Guderley[3] for the nonlifting case, and by Cole and Messiter[4] and Ashley and Landahl[5] for the more general case with lift. Basic to the cited works[2–5] is a field structure composed of two distinct regions: an inner region similar to that in the classical slender-body (Jones/Ward/Adams and Sears) theory,[6–8] and an axisymmetric outer region governed by the transonic smalldisturbance equation. The same field model has been employed recently by Stahara and Spreiter[9] in which configurations of unit-order aspect ratio were considered.

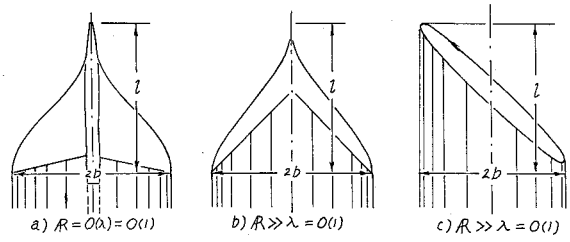

Fig. 1 Examples of configurations studied.

This Note is concerned with the basic structure of three-dimensional transonic flows around configurations having finite (nonvanishing) leading-edge sweep angles. Refer to Fig. 1 for examples. We should like to point out that, unlike the field model stipulated in Refs. 2–5 and 9, the inviscid transonic small-disturbance regime admits three domains, representing different degrees of asymmetry controlled by the lift. Only in the domain where the lift contribution is relatively small will the area rule be applicable and, even in this case, its corrections are not all together negligible.

Basic to the present study are the parameters λ, τ, and α characterizing, respectively, the leading-edge angle of the planform, the configuration thickness ratio, and a degree of asymmetry associated with the lift or the side force. For the class of configurations of interest, these parameters may be defined as

$$\lambda \equiv b/l, \quad \tau \equiv S_{\max}/bl, \quad \alpha \equiv F_{\max}/\rho_\infty U_\infty^2 b^2 \tag{1}$$

where b is the half span, and l an over all length, $S_{\max}$ the maximum cross-sectional area and $F_{\max}$ the maximum integrated lateral force. For a Concorde-type planform, such as that of a in Fig. 1, λ is comparable to the classical aspect ratio $AR \equiv 4b^2/$(planform area). On the other hand, for a swept or yawed wing of high aspect ratio, such as that of b or c in Fig. 1, λ will be very much smaller than AR. Note that τ and α give the thickness ratio and incidence for the configuration as a whole and may be much smaller than the corresponding values characterizing a local wing section. The frame work of our analysis is then defined by

$$|M_\infty - 1| \ll 1, \quad \tau \ll 1, \quad \alpha \ll 1, \quad \lambda = 0(1) \tag{2}$$

So long as $\lambda = 0(1)$, the theory admits low as well as high aspect ratio wings. We assume in the following a steady flow of a calorically perfect gas with a uniform freestream. The perturbation field in this problem can be described by a potential, subject to a relative error comparable to the square of the perturbation velocity.

The Inner flow Region

Let x, y, and z be the Cartesian coordinates with the x axis running parallel to the freestream (occasionally, we may refer y as x_2, and z as x_3). To render the analysis more definite, the solution for the perturbation velocity potential will be written in ascending order of τ and α as (for the inner region)

$$\varphi/Ub = \tau \cdot \ln\varepsilon \cdot g(x) + \tau\varphi_\tau + \alpha\varphi_\alpha + \dots \tag{3}$$

where the logarithm of a small parameter ε is anticipated to arise from the matching with the outer solution and will be determined in the course of the analysis. The set of reduced variables which will remain at unit order in the inner region consists of $\tilde{x} = x/l$, $\tilde{y} = y/b$, $\tilde{z} = z/b$, g, φ_τ, φ_α, $\tilde{S} = S/\tau bl$ and $\tilde{f}_j = F_j/\alpha\rho_\infty U^2 b^2$, with $j = 2$ or 3. In terms of these reduced variables, the partial differential equation governing the inner

Received March 6, 1972; revision received March 28, 1972. The work is supported by the Office of Naval Research, Contract N00016-67-A-0269-0021.

Index categories: Aerodynamic and Powerplant Noise (Including Sonic Boom); Aircraft Configuration Design.

* Professor, Division of Engineering and Applied Mechanics. Member AIAA.

† Research Assistant, Division of Engineering and Applied Mechanics.